Scaling Relations for the Lengths and Widths of Fractures

T. Walmann, A. Malthe-Sørenssen, J. Feder, T. Jøssang, and P. Meakin
Department of Physics, University of Oslo, P.O. Box 1048, Blindern, N-0316 Oslo, Norway
and Fracton a.s., Tåsenveien 74C, N-0873 Oslo, Norway

H. H. Hardy
Conoco Inc., P.O. Box 1267, Ponca City, Oklahoma 74603
(Received 8 July 1996)

Fault-fracture patterns have been studied in slabs of clay during extensional deformations. Fractures nucleate and grow on many scales. A new scaling relation is proposed for the length l of a fracture as a function of the area $l \sim A^{\beta}$, with the same exponent $\beta = 0.68 \pm 0.03$ for many deformation types. A consequence of this scaling relation is that the width of a fracture scales with the length as $w \sim l^{(1-\beta)/\beta}$. A spring network model is shown to reproduce the pattern, both visually and statistically, with the same scaling exponents. [S0031-9007(96)01718-8]

PACS numbers: 62.20.Mk, 61.43.–j, 64.60.–i, 81.40.Np

Since the pioneering work of Mandelbrot *et al.* [1] more than a decade ago, the self-affine roughness of fractured surfaces has been studied in many materials [2–5]. This has led to the idea that the Hurst exponent is a universal, material independent characteristic [5,6]. However, others have attempted to correlate the Hurst exponent with material properties, including the toughness [4,6]. While the self-affine scaling of fracture surfaces appears to be well established, the universality of the Hurst exponent remains controversial.

Most of the work on the scaling of fracture processes has been focused on the propagation of a single crack and has stimulated the development of new theoretical approaches to crack growth. In practice, the spanning fracture may be accompanied by smaller cracks and branches that are not detected, or are overlooked. In many materials, failure occurs as a result of the growth and coalescence of a large number of cracks. This is particularly true in the failure of complex, disordered materials such as rock and concrete. Knowledge of the distribution of shapes and sizes of cracks provides an opportunity to study other aspects of the failure process that may also show universal scaling behavior and lead to a better understanding of failure in an important class of materials. The structure of fault patterns is also important in oil reservoir characterization, in particular in order to predict the fracture pattern at subseismic scales.

The use of small physical scale models to study large scale geological structures has a history going back to at least the 16th century [7]. Clay appears to have the right combination of rheological properties to study the folding of sedimentary rocks, and has been used for this purpose for more than 150 years [8–10]. Experiments with small scale models have had an important influence on the development of the understanding of tectonics [11], diapirism, and other processes. However, there has been little effort to study the morphologies generated by clay models in quantitative terms. Some progress has been made towards understanding more complex fracture patterns in thin films in terms of model experiments [12] and simulations [13], but no new relations have been proposed to characterize the shape of fractures.

Fracture patterns in clay have been simulated using purely statistical models [14]. More realistic results have been obtained using physically based models. Based on ideas from the study of disordered systems, materials have been modeled on a mesoscopic scale as networks of springs [15–17] or beams [18]. In particular, drying cracks in thin films have been simulated as thermally induced cracks in a spring network connected to a substrate [19]. Also, a random fuse network model has been proposed as a model for clay cracking during drying [20]. However, there have not been any quantitative comparisons between models and experiments.

We have studied the surface fracturing of clay in several deformation modes inspired by practical problems from oil reservoir engineering. We propose a scaling relation for a new set of measurable quantities characterizing the length and width of a fracture. The exponents are robust: independent of the clay type, moisture content, the type of extensional deformation, and the deformation speed, within certain limits. We have constructed a physically based network model that displays convincing visual and a quantitative statistical correspondence with the experiments.

Experiments.—Four different experimental setups were used: two for localized extension (A and B) and two for uniform extension (C and D), as explained in Fig. 1. Three ordinary pottery clays were used: the stoneware clays 1161/Y, St. Thomas White from Potclays Ltd. (UK), and the porcelain clay, HPB-45937, from KPCL (NL). Experiments with different moisture contents were performed for the 1161/Y clay. The moisture content was measured in terms of the density [10] and varied in the range $1.81–1.93\ \mathrm{g/cm^3}$. Wet clay appeared to be more

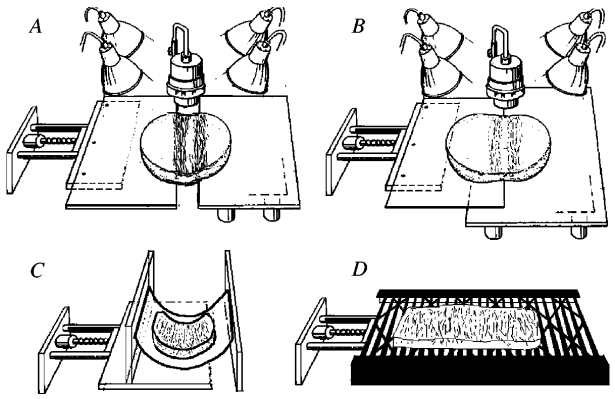

FIG. 1. Clay deformation experiments. In setup A the clay slab initially rested on two 10 mm thick wooden plates of size 50×25 cm in contact with each other. The two plates were driven apart by a motor, forcing the clay to deform, since it did not slip on the plates. The clay sunk down into the 10 mm thick gap created in the opening between the plates. Setup B consisted of a 0.4 mm motorized aluminum plate on top of a stationary wooden plate. Setup C used a bent metal plate. The clay slab was prepared inside the concave part of the plate which was then straightened leading to uniform extension of the top of the slab. Setup D was based on the idea of Oertel [21] using a scissor mechanism with multiple shears. Each shear had upright pins and was moved by a motor. *U*-shaped metal profiles rested on the pins, leading to a uniform shortening or lengthening of the base as the motor moved the scissor mechanism.

ductile than drier clays. When water was added the fractures changed from brittle open cracks to more fault-like displacements. We characterized the shape of a fracture using the projection onto a horizontal plane as seen when looking at the fracture from above. With this definition the shape did not change with the moisture content in the range investigated. Deformation speeds were varied in the range $4-110$ μm/sec for setup B while for the other experiments only one speed was used (53 μm/sec). The width of the fracture zone increased with deformation speed, but the shapes and statistics of the fractures remained the same.

The samples were prepared by forming the shape of the slab and the top surface by hand. Small amounts of water were used to smooth the surface. The excess water was removed and the final shape was obtained by gently smoothing the surface with a putty knife. Finally, to enhance the visual contrast, the surface was colored with carbon black using a soft brush. A typical size for the clay slab was 25×25 cm with a thickness of 25 mm. Digital images of the top surface of the clay models were recorded with a high resolution CCD camera system (Photometrics Series-200 w/Kodak KAF-4200 with 2000×2000 pixels). In experiments with setups A, B, and D of Fig. 1 images were recorded every 40 s. With setup C it was possible to obtain focused pictures only at the final stage when the metal plate and the top surface of the clay were flat.

A fracture appeared as a gray opening in the black surface. The areas corresponding to open fractures were found from the digital pictures: A fracture was defined as a connected region of pixels in the picture with an intensity higher than a certain threshold. At the resolution used, the detected fractures corresponded very closely to the fractures found by careful visual inspection of the clay surface. Pictures were taken at different resolutions, but the basic statistical relationships did not vary with the resolution.

For very small extensions the clay surface did not fracture, but fractures nucleated and grew as the extension increased. The growth of a fracture was halted either because of shielding by other fractures or because it encountered a particularly strong region in the clay. We observed that long fractures frequently appeared when two or more fractures joined at their ends. Figure 2(a) shows an example of the fracture pattern for setup C in Fig. 1. Fractures appear on all scales. Many important correlations are evident: Large fractures often have smaller fractures near their ends. What may be perceived as one long fracture is often a collection of smaller, aligned fractures. From close inspection of the clay slab, it was found that these fractures were not connected on the surface. The actual surface deformation was of two types: fault deformations, mostly oriented in the same direction, and open surface cracks. Most detected fractures were from faults in the clay; the detected fracture area was then the projection of the open fault onto the surface plane.

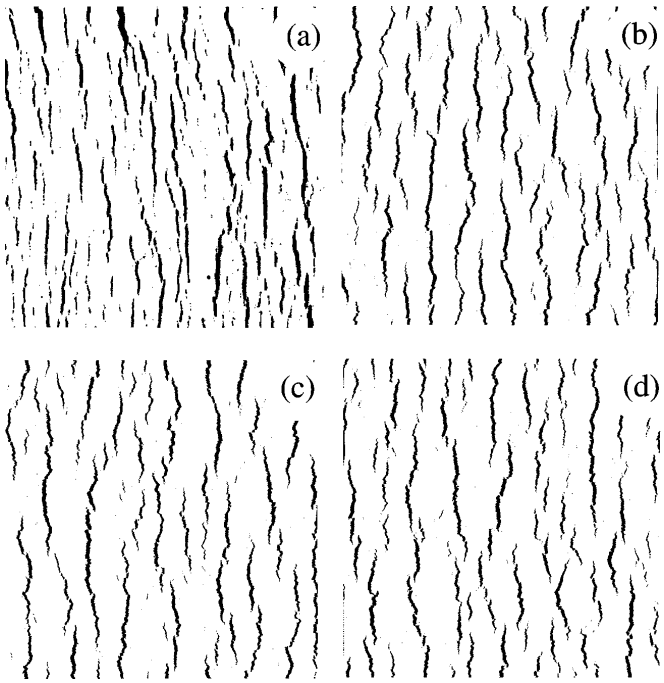

FIG. 2. (a) A 2000×2000 pixels picture from an experiment with setup C of Fig. 1 at 18% deformation is compared with patterns simulated using a 500×500 network at 15% uniform extension in the x direction. Different statistical realizations are shown in (b), (c), and (d). The simulations are for $a = 1.15$ and $\triangle a = 0.05$.

Simulations.—The deformation and fracturing of the clay slab was modeled as a network of elastic springs connected to a substrate [19]. This represents the clay on an intermediate scale, between the microscopic details of the clay particles and the macroscopic behavior of the whole slab. The clay surface is represented as a two-dimensional triangular network of nodes connected by springs each with spring constant $k_1 = 1$. The coupling from the substrate through the height of the clay slab is represented by weaker springs with spring constants k_2. During deformation, the substrate attachment points are moved, imposing a deformation on the surface layer.

Disorder is an essential component of the model and the physical system: It is introduced by a distribution of breaking thresholds for the springs. It was assumed that each spring in the network can sustain only a certain maximum force m_i, randomly selected from a normal distribution with average a and variance $\triangle a^2$.

Substrate deformation proceeds in small steps δx. All substrate positions are moved and the lattice relaxed into a state of minimal energy (zero net force on each node) using overrelaxation [22]. The spring in which the force exceeds its threshold m_i by the largest amount is removed and the lattice is relaxed again. This procedure is iterated until all bonds are below their thresholds. The substrate is then further deformed by δx and the breaking process is repeated. Fractures appear as open connected areas in the surface.

The mechanical coupling to the substrate introduces a length scale—the average distance between fractures, λ. In a one-dimensional system λ scales as $k_2^{-1/2}$ for small k_2 [20,23], and a similar dependence was found in two dimensions.

The pattern from the simulation depended on the choice of parameters. For large k_2 (10^{-1}) the fracture pattern consisted of many small fractures; as k_2 decreased the global effects became more important and the fractures looked more similar to the clay fractures. The choice of threshold distribution was also important. However, we found that most centralized, symmetric distributions such as uniform and Weibull distributions with realistic parameters, gave similar results. In the simulations presented here a normal distribution was used.

For a reasonable set of parameters, the evolution of the fracture patterns in the simulations was quite similar to that of the experiments with similar nucleation dynamics and coalescence dynamics. For a normal distribution of the threshold forces with $a = 1.15$ and $\triangle a = 0.05$, and $k_2 = 10^{-3}$ the patterns at 15% extension compare well with the experimental pattern as is shown in Fig. 2.

Since the fractures (see Fig. 2) are oriented within $\pm 5°$ of the vertical direction (the direction perpendicular to the extension), we define the length of a fracture, l, as the vertical distance from the upper to the lower end of the fracture, and the width, w, as the average horizontal width of the fracture aperture. Thus $A = lw$ is the observed area of the fracture. Figure 3 shows that $l \sim A^{\beta}$ for both experiments and simulations. The average width scales with the area as $w \sim A^{1-\beta}$. An upper cutoff is given by the system size. To avoid size dependent effects in the experiments only the central region of the slab was analyzed removing the fractures extending outside this region. For the simulations periodic boundary conditions in the vertical direction were used. Systematic deviations from scaling are observed for small fractures. In the experiments this is an artifact of the digitalization process. At higher resolutions small fractures also obey the scaling law. In the simulation the deviation is also a result of finite resolution since a broken bond is the lower limit of fracture width.

The scaling behavior of the experimental data extends over three orders of magnitude for the lengths and four for the areas. The scaling seems to be independent of the clay type, moisture content, history, speed, and extension type used. An interesting observation is that β appears to decrease with increasing deformation. This can be seen in Fig. 4 where β is plotted as a function of the percentage of the imaged area that belongs to fractures, i.e., the percentage of black pixels to the total number of pixels in Fig. 2(a). However, the quality of the experimental data is not good enough to determine the dependence in detail. For small deformation only a few small fractures are present. The statistics are poor and dominated by the smallest fractures whose lengths grow linearly with the area due to the finite and discrete width. The exponents found for small deformations are effective exponents resulting from the crossover from the linear dependence at small extensions to the power-law dependence found for larger extensions. For very large extensions the fractures

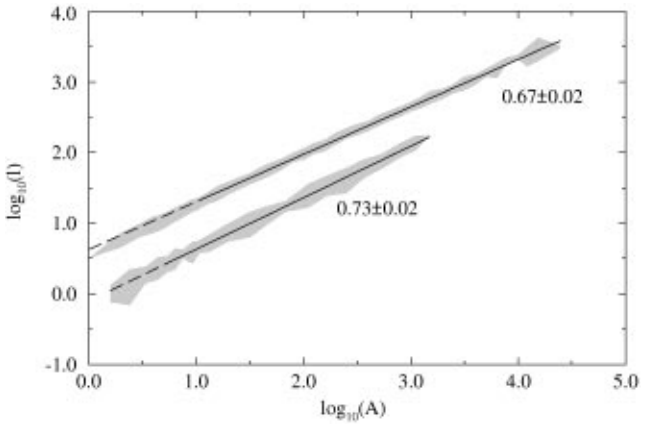

FIG. 3. Plots of l as a function of A for the ≈3000 fractures in the experimental picture shown in Fig. 2(a) and for a simulation on a 800 × 800 network at 15% extension. The experimental data have been shifted upwards by a factor of $10^{0.5}$. The solid part of the fitted lines indicates the region over which the fit was performed. The shaded area indicates one standard deviation of the observed length l for given A, to each side of the average length. The exponents are equal within the statistical uncertainties.

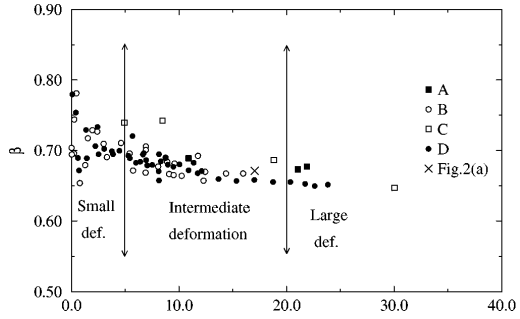

FIG. 4. The exponent β from experiments of type A, B, C, and D as a function of the percentage of fractured area to the total area imaged. Three different regions are indicated. In the small and large deformation regions there are bad statistics. For the intermediate region the statistics are very good. A decrease of β is observed with increasing deformation.

started to interconnect and span the whole system and the behavior changed. In the intermediate region as indicated in Fig. 4 an average value is given by $\beta = 0.68 \pm 0.03$.

The scaling laws $l \sim A^{\beta}$ and $w \sim A^{1-\beta}$ imply that the large fractures are relatively thinner than the small fractures:

$$w \sim l^{(1-\beta)/\beta} \sim l^{(0.32\pm0.03)/(0.68\pm0.03)} \sim l^{0.47\pm0.03}. \quad (1)$$

The scaling of the width as a function of the length through the scaling of the area gives better statistics than a direct determination.

In conclusion, quantitative measurements on a traditional geological model system have been used to establish new scaling relations for the lengths and widths of fractures. We find that $l \sim A^{0.68\pm0.03}$ and $w \sim l^{0.47\pm0.03}$, independent of the experimental parameters. However, a dependence on the amount of extension is observed. The exponent β appears to decrease with increasing extension.

The very good correspondence both visually and statistically between simulations and experiments is surprising, since the main fracture process in the clay is three-dimensional faulting, whereas the model is strictly two dimensional. However, the excellent correspondence suggests that the surface fractures in clay can be understood from a simple surface cracking model and gives confidence in the use of such models to study the fracturing of clay materials.

We gratefully acknowledge the financial support of the Norwegian Research Council. We thank B. B. Mandelbrot for an enlightening discussion. This work has received support from the Norwegian Research Council (Program for Supercomputing) through a grant of computing time.

[1] B. B. Mandelbrot, D. E. Passoja, and A. J. Paullay, Nature (London) 308, **721** (1984).
[2] R. H. Dauskardt, F. Haubensak, and R. O. Ritchie, Acta Metall. Mater. **38**, 143 (1990).
[3] B. L. Cox and J. S. Y. Wang, Fractals **1**, 87 (1993).
[4] P. Meakin, Phys. Rep. **235**, 189 (1993).
[5] K. J. Måløy, A. Hansen, E. L. Hinrichsen, and S. Roux, Phys. Rev. Lett. **68**, 213 (1992).
[6] E. Bouchaud, G. Lapasset, and J. Planès, Europhys. Lett. **13**, 73 (1990).
[7] *The Deformation of the Earth's Crust*, edited by W. H. Bucher (Princeton University Press, Princeton, New Jersey, 1941).
[8] H. Cloos, Centralbl. Mineral. Pal. **5**, 609 (1928).
[9] H. Cloos, Naturwissenschaften **34**, 741 (1930).
[10] G. Oertel, Tectonophysics **2**, 343 (1965).
[11] V. V. Belousov and M. V. Gzovsky, in *Physics and Chemistry of the Earth*, edited by L. H. Ahrens, F. Press, S. K. Runcorn, and H. C. Urey (Pergamon Press, Oxford, 1965), pp. 409–499.
[12] A. Skjeltorp and P. Meakin, Nature (London) **335**, 424 (1988).
[13] Y. Termonia and P. Meakin, Nature (London) **320**, 429 (1986).
[14] H. J. Herrmann and S. Roux, *Statistical Models for the Fracture of Disordered Media* (North-Holland, Amsterdam, 1990).
[15] S. Feng and P. N. Sen, Phys. Rev. Lett. **52**, 216 (1984).
[16] Y. Kantor and I. Webman, Phys. Rev. Lett. **52**, 1891 (1984).
[17] P. M. Duxbury, P. L. Leath, and P. D. Beale, Phys. Rev. B **36**, 367 (1987).
[18] S. Roux and E. Guyon, J. Phys. (Paris), Lett. **46**, L999 (1985).
[19] P. Meakin, Thin Solid Films **151**, 165 (1987).
[20] H. Colina, L. de Arcangelis, and S. Roux, Phys. Rev. B **48**, 3666 (1993).
[21] G. Oertel, Geotimes **6**, 26 (1962).
[22] D. M. d. G. Allen, *Relaxation Methods* (McGraw-Hill, New York, 1954).
[23] O. Morgenstern, I. M. Sokolow, and A. Blumen, Europhys. Lett. **22**, 487 (1993).